1989ApJ...337..306A

THE ASTROPHYSICAL JOURNAL, 337:306–317, 1989 February 1
© 1989. The American Astronomical Society. All rights reserved. Printed in U.S.A.

COLLISIONAL RATE COEFFICIENTS OF C_3H_2 AND THE DETERMINATION OF PHYSICAL CONDITIONS IN MOLECULAR CLOUDS

L. W. AVERY
Herzberg Institute of Astrophysics, National Research Council of Canada
AND
SHELDON GREEN
NASA/Goddard Space Flight Center, Institute for Space Studies
Received 1988 May 17; accepted 1988 July 12

ABSTRACT

Collisional excitation rates for C_3H_2, calculated using the coupled states approximation, are presented. These rates are used in statistical equilibrium calculations to evaluate the potential of C_3H_2 rotational spectral lines as diagnostic probes of physical conditions in molecular clouds. C_3H_2 produces a number of spectral line pairs, whose members are close together in frequency but arise from levels with different excitation energies. The brightness temperature ratio of such a line pair is independent of systematic observational errors but is sensitive to variations in density and radiative trapping in molecular clouds. The calculated dependence of brightness temperature ratio upon H_2 density and C_3H_2 abundance is presented for a number of line pairs for a simple, homogeneous cloud under the large velocity gradient radiative transfer model. Among the more useful pairs for diagnostic purposes are 1_{10}–1_{01}, 2_{20}–2_{11} (18343 MHz, 21587 MHz), 2_{12}–1_{01}, 3_{12}–3_{03} (85, 339 MHz, 82966 MHz), 2_{12}–1_{01}, 2_{02}–1_{11} (85339 MHz, 82094 MHz), and 4_{14}–3_{03}, 4_{04}–3_{13} (150852 MHz, 150821 MHz).

Subject headings: interstellar: molecules — molecular processes — transition probabilities

I. INTRODUCTION

The recently identified astrophysical molecule, C_3H_2 (cyclopropenylidene) has been shown to be widespread and readily observable in a variety of sources (Matthews and Irvine 1985; Matthews *et al.* 1986; Seaquist and Bell 1986). This molecule is an asymmetric top with a large dipole moment of 3.4 debye (Brown, Godfrey, and Bettens 1987; Kanata, Yamamoto, and Saito 1987) and a *b*-type spectrum. It has two equivalent, off-axis H nuclei, and the resultant spin statistics give rise to *ortho* and *para* symmetry species with relative statistical weights in the ratio of 3:1.

The molecular constants and ground-state rotational spectrum of C_3H_2 are accurately known, and there are a good number of spectral lines distributed throughout the observable microwave region (Thaddeus, Vrtilek, and Gottlieb 1985; Bogey *et al.* 1987). The existence of numerous spectral transitions corresponding to a range of excitation energies, and the strengths of these lines in numerous sources, suggest that C_3H_2 is potentially a useful molecule for probing the physical conditions in objects where it is observed. In particular, a number of groups or pairs of lines have similar frequencies, but correspond to different excitation energies. Examples are the 1_{10}–1_{01} and 2_{20}–2_{11} lines at 18343 and 21587 MHz (excitation energies E/k of 0.9 and 9.7 K, respectively) and the 2_{12}–1_{01}, 2_{02}–1_{11} lines at respective frequencies and excitation energies of 85339 and 82094 MHz and 4.1 and 6.4 K. Numerous other combinations can be found in Table 1 of the paper by Thaddeus, Vrtilek, and Gottlieb (1985). The ratio of line strengths for such pairs should in principle be sensitive, through excitation effects, to the H_2 number density $N(H_2)$ in the clouds where the lines are observed. The advantage of using such a ratio for diagnostic purposes is that the two lines can be observed almost simultaneously with the same telescope. Subsequently, in forming the ratio of line strengths, systematic errors involving source coupling efficiency, calibration uncertainty, and atmospheric absorption are canceled out.

To determine the manner in which various C_3H_2 line strengths and ratios depend upon excitation conditions, the collisional excitation rates are required. Green, DeFrees, and McLean (1987) have calculated rate coefficients for C_3H_2 in collisions with He atoms at temperatures from 30 to 120 K. However, many of the sources in which C_3H_2 is strongest are cold, dark clouds characterized by a temperature of about 10 K. We report in § II the results of new calculations of rate coefficients at temperatures of 10–30 K, which should be more suitable for cold, dark cloud analysis than the higher temperature results. The excitation rates at 10 and 30 K are used in statistical equilibrium calculations to illustrate the excitation properties and density-dependent behavior of various C_3H_2 line ratios.

II. CALCULATION OF THE COLLISIONAL EXCITATION RATES

The excitation rates presented by Green, DeFrees, and McLean (1987) were obtained from an accurate theoretical intermolecular potential using the infinite-order sudden (IOS) approximation for molecular collision dynamics. The IOS method greatly simplifies the scattering calculation at the cost of ignoring rotational energy spacings compared with the collisional kinetic energy. It is thus expected to be most accurate at higher collision energies and, hence, higher temperatures. Accuracy of the IOS approximation for this system was tested in the earlier study by comparison with more accurate coupled states (CS) calculations which properly include rotational energies. Comparisons were done for only one collision energy, corresponding to about 60 K, at which the IOS approximation was found to be reasonably good, within about 50% of CS values for the larger, more important cross sections. Its utility below about 30 K, however, seemed doubtful.

© American Astronomical Society • Provided by the NASA Astrophysics Data System

1989ApJ...337..306A

TABLE 1A

RATE CONSTANTS FOR *Ortho* C_3H_2
(10^{-11} cm^{-3} s^{-1})

Temperature = 10 K

initial \ final	$1_{0,1}$	$1_{1,0}$	$2_{1,2}$	$2_{2,1}$	$3_{0,3}$	$3_{1,2}$	$3_{2,1}$	$4_{1,4}$	$3_{3,0}$	$4_{2,3}$	$5_{0,5}$	$4_{3,2}$	$4_{4,1}$	$5_{1,4}$	$6_{1,6}$	$5_{2,3}$
$1_{0,1}$	...	0.80	4.18	2.74	0.24	0.52	0.53	1.03	0.11	0.07	0.13	0.11	0.13	0.03	0.01	0.00
$1_{1,0}$	0.87	...	1.03	0.94	3.98	0.32	0.04	0.11	0.90	0.48	0.05	0.03	0.02	0.01	0.05	0.02
$2_{1,2}$	3.77	0.86	...	2.98	0.84	1.38	0.46	0.43	0.36	0.05	0.61	0.17	0.11	0.03	0.02	0.01
$2_{2,1}$	3.23	1.02	3.88	...	1.04	1.74	0.57	1.78	0.35	0.10	0.17	0.18	0.26	0.20	0.02	0.01
$3_{0,3}$	0.27	4.13	1.05	1.00	...	0.57	0.44	0.44	1.89	1.12	0.11	0.06	0.12	0.02	0.30	0.08
$3_{1,2}$	0.87	0.49	2.57	2.50	0.84	...	2.43	1.05	1.05	0.44	1.13	0.90	0.29	0.17	0.03	0.03
$3_{2,1}$	1.12	0.08	1.07	1.01	0.80	3.00	...	2.64	0.63	0.49	0.32	1.18	0.51	0.72	0.03	0.06
$4_{1,4}$	1.88	0.18	0.87	2.75	0.70	1.13	2.31	...	0.23	0.31	0.37	0.37	0.52	0.70	0.06	0.02
$3_{3,0}$	0.27	1.95	0.94	0.71	3.97	1.48	0.72	0.30	...	3.60	0.37	0.28	0.22	0.05	0.17	0.43
$4_{2,3}$	0.21	1.41	0.19	0.28	3.16	0.84	0.75	0.55	4.85	...	0.84	0.64	0.32	0.23	0.86	0.75
$5_{0,5}$	0.46	0.17	2.44	0.52	0.36	2.41	0.55	0.74	0.56	0.95	...	1.67	0.24	0.25	0.30	0.18
$4_{3,2}$	0.52	0.12	0.92	0.73	0.26	2.59	2.73	0.99	0.58	0.97	2.24	...	2.23	0.58	0.06	0.21
$4_{4,1}$	0.86	0.13	0.83	1.46	0.67	1.13	1.61	1.88	0.61	0.67	0.45	3.06	...	1.91	0.21	0.21
$5_{1,4}$	0.20	0.07	0.26	1.25	0.12	0.74	2.57	2.89	0.17	0.53	0.53	0.89	2.16	...	0.77	0.19
$6_{1,6}$	0.07	0.42	0.18	0.13	2.32	0.14	0.14	0.29	0.62	2.32	0.71	0.10	0.28	0.89	...	1.22
$5_{2,3}$	0.06	0.23	0.11	0.06	0.90	0.26	0.38	0.14	2.34	3.06	0.66	0.57	0.41	0.33	1.84	...

Temperature = 20 K

initial \ final	$1_{0,1}$	$1_{1,0}$	$2_{1,2}$	$2_{2,1}$	$3_{0,3}$	$3_{1,2}$	$3_{2,1}$	$4_{1,4}$	$3_{3,0}$	$4_{2,3}$	$5_{0,5}$	$4_{3,2}$	$4_{4,1}$	$5_{1,4}$	$6_{1,6}$	$5_{2,3}$
$1_{0,1}$	...	0.88	4.53	3.35	0.35	0.88	1.07	2.45	0.26	0.19	0.52	0.46	0.59	0.17	0.06	0.03
$1_{1,0}$	0.92	...	0.90	1.21	5.80	0.44	0.06	0.28	2.00	1.50	0.19	0.10	0.11	0.06	0.35	0.14
$2_{1,2}$	3.33	0.64	...	2.84	1.09	1.99	1.00	0.83	0.62	0.15	1.88	0.56	0.44	0.16	0.10	0.04
$2_{2,1}$	2.82	0.98	3.24	...	0.92	2.58	0.77	2.74	0.57	0.21	0.48	0.49	0.87	0.80	0.08	0.03
$3_{0,3}$	0.25	3.86	1.03	0.76	...	0.63	0.45	0.70	2.52	2.08	0.26	0.14	0.30	0.07	1.20	0.32
$3_{1,2}$	0.75	0.36	2.29	2.61	0.77	...	2.45	1.17	0.95	0.65	1.96	1.63	0.65	0.45	0.10	0.10
$3_{2,1}$	1.01	0.06	1.28	0.86	0.61	2.73	...	2.43	0.64	0.54	0.57	1.93	1.00	1.66	0.09	0.18
$4_{1,4}$	1.91	0.21	0.87	2.54	0.78	1.07	2.01	...	0.22	0.39	0.66	0.56	1.01	1.48	0.16	0.06
$3_{3,0}$	0.26	1.93	0.85	0.68	3.65	1.13	0.68	0.28	...	4.36	0.53	0.41	0.43	0.16	0.47	1.28
$4_{2,3}$	0.20	1.49	0.20	0.26	3.08	0.79	0.59	0.51	4.46	...	0.82	0.70	0.41	0.38	1.58	1.57
$5_{0,5}$	0.52	0.18	2.52	0.57	0.38	2.28	0.60	0.84	0.52	0.79	...	1.70	0.30	0.35	0.52	0.29
$4_{3,2}$	0.59	0.12	0.96	0.74	0.26	2.43	2.59	0.92	0.52	0.86	2.17	...	2.46	0.81	0.10	0.36
$4_{4,1}$	0.88	0.16	0.89	1.53	0.64	1.13	1.57	1.93	0.63	0.59	0.44	2.88	...	2.07	0.28	0.28
$5_{1,4}$	0.24	0.08	0.31	1.35	0.14	0.75	2.51	2.71	0.22	0.53	0.51	0.91	1.98	...	0.73	0.27
$6_{1,6}$	0.08	0.47	0.19	0.14	2.43	0.17	0.13	0.30	0.65	2.17	0.75	0.11	0.27	0.72	...	1.39
$5_{2,3}$	0.06	0.26	0.10	0.06	0.87	0.23	0.36	0.15	2.40	2.88	0.56	0.54	0.36	0.36	1.86	...

© American Astronomical Society • Provided by the NASA Astrophysics Data System

1989ApJ...337..306A

TABLE 1A—*Continued*

Temperature = 30 K

initial	final															
	$1_{0,1}$	$1_{1,0}$	$2_{1,2}$	$2_{2,1}$	$3_{0,3}$	$3_{1,2}$	$3_{2,1}$	$4_{1,4}$	$3_{3,0}$	$4_{2,3}$	$5_{0,5}$	$4_{3,2}$	$4_{4,1}$	$5_{1,4}$	$6_{1,6}$	$5_{2,3}$
$1_{0,1}$	...	0.92	4.55	3.50	0.43	0.99	1.32	3.22	0.36	0.27	0.88	0.79	0.98	0.32	0.11	0.06
$1_{1,0}$	0.94	...	0.81	1.36	6.38	0.46	0.07	0.42	2.61	2.22	0.30	0.15	0.20	0.11	0.71	0.29
$2_{1,2}$	3.13	0.54	...	2.61	1.20	2.20	1.36	1.06	0.72	0.21	2.73	0.84	0.68	0.29	0.18	0.07
$2_{2,1}$	2.63	0.99	2.85	...	0.84	2.99	0.84	3.09	0.64	0.28	0.72	0.70	1.30	1.30	0.15	0.05
$3_{0,3}$	0.26	3.67	1.04	0.66	...	0.66	0.44	0.85	2.73	2.57	0.36	0.19	0.40	0.11	1.96	0.52
$3_{1,2}$	0.67	0.30	2.17	2.69	0.75	...	2.43	1.24	0.88	0.74	2.31	1.97	0.83	0.63	0.18	0.15
$3_{2,1}$	0.96	0.05	1.43	0.81	0.53	2.60	...	2.30	0.65	0.54	0.75	2.23	1.28	2.15	0.12	0.26
$4_{1,4}$	1.89	0.24	0.91	2.41	0.84	1.08	1.85	...	0.23	0.44	0.83	0.64	1.29	1.88	0.24	0.11
$3_{3,0}$	0.27	1.92	0.79	0.65	3.50	0.98	0.68	0.29	...	4.53	0.59	0.46	0.53	0.24	0.70	1.89
$4_{2,3}$	0.19	1.53	0.22	0.26	3.07	0.78	0.53	0.53	4.23	...	0.79	0.70	0.44	0.47	1.95	2.07
$5_{0,5}$	0.57	0.19	2.56	0.62	0.39	2.20	0.66	0.91	0.50	0.72	...	1.72	0.33	0.40	0.67	0.34
$4_{3,2}$	0.64	0.12	0.99	0.75	0.26	2.37	2.49	0.88	0.50	0.80	2.17	...	2.51	0.97	0.13	0.45
$4_{4,1}$	0.88	0.18	0.90	1.57	0.61	1.11	1.59	1.98	0.63	0.56	0.46	2.79	...	2.12	0.33	0.34
$5_{1,4}$	0.26	0.09	0.34	1.42	0.15	0.76	2.44	2.64	0.26	0.54	0.51	0.98	1.93	...	0.69	0.34
$6_{1,6}$	0.09	0.53	0.21	0.15	2.56	0.20	0.13	0.31	0.71	2.13	0.80	0.12	0.29	0.65	...	1.56
$5_{2,3}$	0.06	0.28	0.11	0.07	0.87	0.21	0.35	0.18	2.46	2.90	0.53	0.55	0.37	0.41	2.00	...

At very low temperatures, where few rotational levels are accessible, it is computationally feasible to obtain converged CS cross sections, and we have done such calculations for the present study. In particular, cross sections were obtained among all rotor levels lying below 30 cm^{-1}, i.e., 17 *para* levels and 16 *ortho* levels. Calculations were done for a number of total (i.e., rotor plus collision) energies sufficient to obtain thermal averages to 30 K; in particular, $E = 2(1), 16(2), 30, 35, 40, 50, 60, 75$, and 90 cm^{-1}, where the numbers in parentheses indicate the size of the steps in energy between the values not parenthesized. Except at the lowest energies, 30 *para* and 30 *ortho* levels were included in the basis sets. While this does not represent all open channels at the highest energies, it should provide reasonable convergence among the levels for which rates were obtained. All calculations used the MOLSCAT computer code, with numerical tolerances chosen to give cross sections accurate to better than 1%. Rate constants, obtained by averaging the resulting cross sections over thermal velocity distributions, are presented in Table 1.

These CS results provide a more extensive test of IOS values than was possible in the previous work. In particular, CS rates at 30 K are compared in Figure 1 with the earlier IOS values. Agreement here is somewhat less good, as expected, than it was at the higher energy compared previously by Green, DeFrees, and McLean (1987). It is encouraging, however, that the simpler IOS method gives at least a qualitatively correct description, even at this very low temperature.

III. THE STATISTICAL EQUILIBRIUM AND RADIATIVE TRANSFER PROBLEMS

Many of the dark cloud sources where C_3H_2 has been observed show strong lines, indicating that they are probably optically thick. Consequently, it is necessary to incorporate the effects of radiative trapping into the excitation calculations. This has been done, for the results presented here, by using the large velocity gradient (LVG) approximation for a collapsing, spherical cloud of uniform density, as discussed by Goldreich and Kwan (1974). Such a model may not be directly applicable to many of the dark clouds which have been observed, but it does provide a relatively simple means of incorporating radiative trapping for illustrative purposes.

The standard equations of statistical equilibrium were solved consistently with the radiative transfer model by iteration. Solutions were obtained for kinetic temperatures (T_k) equal to 10 and 30 K over wide ranges of $N(H_2)$ and the quantity $X/(dV/dR)$ (hereafter denoted by x), where X is the abundance of C_3H_2 relative to H_2 and dV/dR is the velocity gradient within the source. For a given value of T_k, the quantities $N(H_2)$ and x are the only two independent variables for the LVG modeling used here. For $T_k = 10$ K, the statistical equilibrium calculations included the lowest 24 *ortho* levels (i.e., up to level 6_{52}, with $E/k = 65$ K) and 17 *para* levels (up to level 5_{33}, with $E/k = 42$ K). For the *ortho* calculations, the data of Table 1 for the lowest 16 levels were extended to 24

© American Astronomical Society • Provided by the NASA Astrophysics Data System

1989ApJ...337..306A

TABLE 1B

RATE CONSTANTS FOR *Para* C_3H_2
(10^{-11} cm^{-3} s^{-1})

Temperature = 10 K

initial \ final	$^0_{0,0}$	$^1_{1,1}$	$^2_{0,2}$	$^2_{1,1}$	$^2_{2,0}$	$^3_{1,3}$	$^3_{2,2}$	$^3_{3,1}$	$^4_{0,4}$	$^4_{1,3}$	$^5_{1,5}$	$^4_{2,2}$	$^4_{3,1}$	$^4_{4,0}$	$^5_{2,4}$	$^6_{0,6}$	$^5_{3,3}$
$^0_{0,0}$	...	1.60	0.73	0.00	2.58	3.42	0.00	0.16	0.13	0.00	0.04	0.09	0.00	0.11	0.00	0.04	0.06
$^1_{1,1}$	0.68	...	4.88	1.37	0.65	0.30	0.42	0.74	1.10	0.02	0.12	0.11	0.02	0.03	0.02	0.01	0.01
$^2_{0,2}$	0.28	4.34	...	2.28	1.27	0.72	1.42	0.73	0.40	0.07	0.61	0.18	0.09	0.11	0.04	0.02	0.01
$^2_{1,1}$	0.00	1.53	2.85	...	0.83	0.62	2.30	1.16	1.50	0.18	0.19	0.12	0.31	0.03	0.24	0.01	0.01
$^2_{2,0}$	1.36	0.81	1.77	0.92	...	5.34	0.74	0.44	0.14	1.36	0.12	0.08	0.02	0.39	0.02	0.09	0.09
$^3_{1,3}$	1.63	0.33	0.91	0.63	4.84	...	0.69	0.56	0.45	1.07	0.12	0.08	0.06	0.33	0.02	0.30	0.09
$^3_{2,2}$	0.00	0.71	2.67	3.47	1.00	1.03	...	2.41	1.21	0.50	1.16	0.72	0.37	0.16	0.15	0.02	0.01
$^3_{3,1}$	0.15	1.65	1.84	2.32	0.80	1.12	3.21	...	2.98	0.43	0.31	1.01	0.27	0.23	0.61	0.05	0.03
$^4_{0,4}$	0.10	1.98	0.82	2.42	0.20	0.72	1.30	2.40	...	0.31	0.41	0.40	0.53	0.07	0.67	0.06	0.02
$^4_{1,3}$	0.00	0.05	0.24	0.52	3.47	3.02	0.93	0.61	0.55	...	0.86	0.62	0.34	1.63	0.22	0.79	0.61
$^5_{1,5}$	0.06	0.44	2.45	0.59	0.35	0.39	2.46	0.49	0.81	0.97	...	1.53	0.27	0.41	0.23	0.28	0.20
$^4_{2,2}$	0.18	0.53	0.94	0.51	0.31	0.34	1.98	2.10	1.02	0.91	2.01	...	2.08	0.91	0.63	0.08	0.42
$^4_{3,1}$	0.00	0.13	0.57	1.58	0.10	0.30	1.25	0.68	1.69	0.62	0.44	2.55	...	0.63	2.45	0.14	0.30
$^4_{4,0}$	0.33	0.17	0.82	0.18	2.16	2.00	0.63	0.68	0.25	3.48	0.77	1.31	0.74	...	0.24	0.39	2.25
$^5_{2,4}$	0.00	0.17	0.33	1.61	0.15	0.12	0.66	2.02	2.73	0.50	0.48	1.00	3.17	0.27	...	0.68	0.17
$^6_{0,6}$	0.14	0.07	0.17	0.10	0.60	2.29	0.11	0.19	0.26	2.15	0.69	0.16	0.21	0.50	0.79	...	1.29
$^5_{3,3}$	0.31	0.13	0.11	0.07	0.97	1.07	0.07	0.16	0.13	2.52	0.72	1.17	0.68	4.31	0.29	1.95	...

Temperature = 20 K

initial \ final	$^0_{0,0}$	$^1_{1,1}$	$^2_{0,2}$	$^2_{1,1}$	$^2_{2,0}$	$^3_{1,3}$	$^3_{2,2}$	$^3_{3,1}$	$^4_{0,4}$	$^4_{1,3}$	$^5_{1,5}$	$^4_{2,2}$	$^4_{3,1}$	$^4_{4,0}$	$^5_{2,4}$	$^6_{0,6}$	$^5_{3,3}$
$^0_{0,0}$	...	1.79	0.72	0.00	3.84	6.20	0.00	0.42	0.35	0.00	0.17	0.33	0.00	0.57	0.00	0.31	0.48
$^1_{1,1}$	0.68	...	4.91	1.61	0.83	0.45	0.91	1.68	2.57	0.05	0.50	0.45	0.09	0.12	0.13	0.06	0.07
$^2_{0,2}$	0.20	3.59	...	2.36	1.07	1.03	2.11	1.25	0.81	0.15	1.87	0.55	0.35	0.37	0.17	0.10	0.05
$^2_{1,1}$	0.00	1.32	2.64	...	0.90	0.58	3.05	1.77	2.37	0.39	0.55	0.33	0.88	0.11	0.94	0.06	0.03
$^2_{2,0}$	1.25	0.72	1.26	0.95	...	5.33	0.78	0.66	0.26	3.00	0.30	0.17	0.05	1.19	0.11	0.40	0.44
$^3_{1,3}$	1.62	0.31	0.97	0.49	4.29	...	0.72	0.66	0.70	1.94	0.28	0.19	0.15	0.92	0.07	1.20	0.41
$^3_{2,2}$	0.00	0.77	2.45	3.16	0.77	0.88	...	2.50	1.24	0.73	2.03	1.27	0.76	0.34	0.42	0.08	0.03
$^3_{3,1}$	0.16	1.64	1.67	2.12	0.76	0.93	2.89	...	2.94	0.48	0.49	1.64	0.48	0.44	1.38	0.14	0.08
$^4_{0,4}$	0.10	1.99	0.85	2.24	0.23	0.78	1.13	2.32	...	0.38	0.68	0.60	0.85	0.12	1.44	0.16	0.07
$^4_{1,3}$	0.00	0.05	0.21	0.49	3.57	2.88	0.88	0.50	0.50	...	0.82	0.70	0.39	2.16	0.36	1.51	1.27
$^5_{1,5}$	0.06	0.50	2.52	0.66	0.34	0.39	2.35	0.49	0.86	0.79	...	1.55	0.35	0.49	0.30	0.52	0.34
$^4_{2,2}$	0.16	0.56	0.94	0.51	0.25	0.35	1.87	2.08	0.97	0.85	1.96	...	2.15	0.93	0.77	0.16	0.71
$^4_{3,1}$	0.00	0.13	0.66	1.48	0.09	0.30	1.23	0.67	1.51	0.52	0.49	2.38	...	0.65	2.72	0.18	0.42
$^4_{4,0}$	0.32	0.18	0.75	0.19	2.07	1.99	0.61	0.67	0.24	3.17	0.74	1.13	0.71	...	0.29	0.55	3.15
$^5_{2,4}$	0.00	0.19	0.34	1.62	0.19	0.14	0.70	2.00	2.64	0.50	0.44	0.88	2.80	0.27	...	0.69	0.22
$^6_{0,6}$	0.16	0.08	0.19	0.10	0.66	2.44	0.13	0.20	0.28	2.06	0.74	0.18	0.19	0.51	0.69	...	1.51
$^5_{3,3}$	0.34	0.13	0.12	0.07	0.96	1.11	0.07	0.15	0.16	2.33	0.65	1.06	0.57	3.94	0.29	2.02	...

© American Astronomical Society • Provided by the NASA Astrophysics Data System

1989ApJ...337..306A

TABLE 1B—*Continued*

Temperature = 30 K

initial \ final	$0_{0,0}$	$1_{1,1}$	$2_{0,2}$	$2_{1,1}$	$2_{2,0}$	$3_{1,3}$	$3_{2,2}$	$3_{3,1}$	$4_{0,4}$	$4_{1,3}$	$5_{1,5}$	$4_{2,2}$	$4_{3,1}$	$4_{4,0}$	$5_{2,4}$	$6_{0,6}$	$5_{3,3}$
$0_{0,0}$	...	1.86	0.70	0.00	4.30	7.41	0.00	0.61	0.51	0.00	0.28	0.49	0.00	0.95	0.00	0.69	1.04
$1_{1,1}$	0.67	...	4.69	1.68	0.90	0.53	1.23	2.19	3.36	0.07	0.86	0.72	0.15	0.20	0.26	0.13	0.13
$2_{0,2}$	0.17	3.21	...	2.37	0.93	1.17	2.40	1.44	1.06	0.20	2.72	0.80	0.58	0.54	0.29	0.19	0.10
$2_{1,1}$	0.00	1.23	2.56	...	0.98	0.56	3.28	2.03	2.68	0.50	0.84	0.46	1.22	0.17	1.48	0.10	0.05
$2_{2,0}$	1.19	0.69	1.04	1.01	...	5.16	0.74	0.76	0.34	3.90	0.39	0.21	0.07	1.73	0.21	0.72	0.76
$3_{1,3}$	1.58	0.31	1.01	0.45	3.99	...	0.73	0.67	0.84	2.38	0.37	0.27	0.21	1.30	0.11	1.97	0.69
$3_{2,2}$	0.00	0.83	2.37	3.01	0.65	0.84	...	2.47	1.24	0.82	2.40	1.54	0.96	0.45	0.62	0.14	0.06
$3_{3,1}$	0.17	1.63	1.56	2.04	0.74	0.84	2.71	...	2.91	0.52	0.59	1.95	0.60	0.54	1.83	0.21	0.12
$4_{0,4}$	0.11	1.96	0.91	2.13	0.26	0.83	1.07	2.29	...	0.42	0.83	0.71	0.99	0.15	1.88	0.23	0.12
$4_{1,3}$	0.00	0.05	0.21	0.47	3.60	2.85	0.86	0.49	0.51	...	0.78	0.74	0.40	2.35	0.45	1.86	1.58
$5_{1,5}$	0.06	0.55	2.56	0.73	0.33	0.40	2.28	0.51	0.91	0.71	...	1.54	0.42	0.52	0.34	0.66	0.40
$4_{2,2}$	0.14	0.58	0.94	0.50	0.22	0.37	1.83	2.11	0.98	0.84	1.93	...	2.13	0.95	0.82	0.24	0.82
$4_{3,1}$	0.00	0.13	0.73	1.42	0.08	0.30	1.22	0.69	1.45	0.48	0.56	2.28	...	0.65	2.72	0.20	0.45
$4_{4,0}$	0.31	0.18	0.71	0.21	2.05	2.00	0.61	0.66	0.24	3.02	0.74	1.08	0.69	...	0.33	0.67	3.43
$5_{2,4}$	0.00	0.21	0.34	1.64	0.23	0.16	0.75	2.01	2.63	0.52	0.44	0.84	2.59	0.29	...	0.69	0.24
$6_{0,6}$	0.19	0.10	0.21	0.11	0.72	2.57	0.16	0.22	0.31	2.03	0.79	0.23	0.18	0.57	0.65	...	1.72
$5_{3,3}$	0.37	0.13	0.14	0.06	0.99	1.16	0.08	0.16	0.19	2.22	0.62	1.01	0.52	3.73	0.30	2.21	...

levels using scaled H_2O rates as discussed by Avery (1987). These scaled H_2O rates are undoubtedly inaccurate for C_3H_2, but, in view of the relatively high excitation energies of the levels involved ($E/k > 44$ K), they should not strongly affect the lower level populations of interest in this study. For $T_k =$ 30 K, the CS rates of Table 1 were augmented using 30 K IOS rates from Green, DeFrees, and Mclean (1987). For the *para* calculations, 22 levels were included (i.e., up to level 6_{24}, with $E/k = 55$ K); for the *ortho* state, 24 levels up to 6_{52} were included. For all calculations, the rates of Table 1 were multiplied by $2^{1/2}$ to compensate for the increased average thermal speed of H_2 over that of He (Green 1980). The rates of Table 1 were computed for C_3H_2–He collisions.

IV. RESULTS AND DISCUSSION

a) Line Intensity Ratios

Figure 2 shows the calculated dependence of the brightness temperature ratio, for a number of C_3H_2 line pairs, upon H_2 density and x (relative abundance divided by the source velocity gradient). For all calculations the theoretical statistical weight ratio of 3:1 for the *ortho* and *para* species was used. The *ortho* states, $J_{K_aK_c}$, are those for which $K_a + K_c$ is odd; the *para* states correspond to even values of $K_a + K_c$. In the figure, X is the C_3H_2 abundance relative to H_2, and dV/dR is the velocity gradient in the molecular cloud. The various line pairs selected for Figure 2 include most of the strongest lines for cloud temperatures ≤ 30 K. Each ratio in Figure 2 is presented for kinetic temperatures of 10 and 30 K and corresponds to spectral lines close together in frequency but possessing different excitation energies. Such conditions should, in principle, produce ratios which are sensitive to different cloud densities and temperatures, while minimizing calibration uncertainties. Table 2 lists the frequencies and excitation energies of the lines included in Figure 2.

i) 1_{10}–1_{01}, 2_{20}–2_{11} (18343 MHz, 21587 MHz)

Probably the most widely observed lines of C_3H_2 to date are the K-band 1_{10}–1_{01} and 2_{20}–2_{11} pair. These lines are of particular observational interest because they are strong in dark clouds (Matthews and Irvine 1985; Matthews *et al.* 1986) and have been observed in a wide variety of sources, including the planetary nebula NGC 7027 (Cox, Güsten, and Henkel 1987) and the galaxy NGC 5128 (1_{10}–1_{01} line only; Seaquist and Bell 1986). The statistical equilibrium calculations indicate rather unusual behavior for these lines. In particular, the 2_{20}–2_{11} line is predicted to be refrigerated, with $T_{ex} < 2.8$ K over a wide range of H_2 densities. Consequently, the line is predicted to appear in absorption against the microwave background for typical dark cloud conditions, and such behavior has been confirmed observationally (Madden *et al.* 1987; Matthews *et al.* 1986). However, the 1_{10}–1_{01} line is calculated to have $T_{ex} >$ 2.8 K for all densities, in contrast to earlier calculations by Avery (1987), who used scaled H_2O collision rates, which indicated that, at low densities, the 1_{10}–1_{01} line would also have

© American Astronomical Society • Provided by the NASA Astrophysics Data System

1989ApJ...337..306A

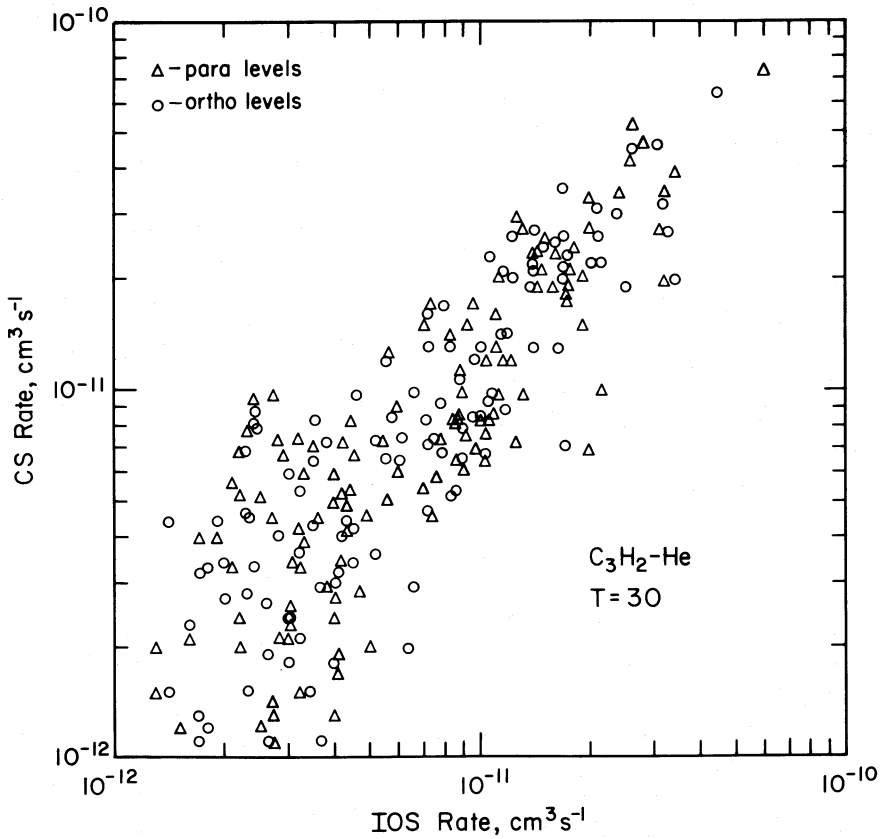

FIG. 1.—Comparison of CS and IOS rate constants at a kinetic temperature of 30 K

$T_{ex} < 2.8$ K. The current results, based on more accurate CS rates for C_3H_2, are undoubtedly more realistic.

At sufficiently high densities, collisions quench the refrigeration of the 2_{20}–2_{11} line, and it should appear in emission. For 10^5 cm^{-3} $\lesssim N(H_2) \lesssim 10^7$ cm^{-3}, both lines have a tendency to be superthermally excited, with $T_{ex} > T_k$ or even negative. As a consequence of this, for $T_k = 30$ K, $N(H_2) \approx 10^6$ cm^{-3}, and relatively large values of x, the 2_{20}–2_{11} line is predicted to be more intense than the 1_{10}–1_{01} line. However, the conditions under which this strength reversal is predicted may seldom be met in molecular clouds. Indications are that warm clouds, with $T_k \approx 30$ K, may not have sufficiently high values of x. For example, the C_3H_2 observations in Orion–KL (Bell *et al.* 1988) suggest that $X \approx 1.5 \times 10^{-9}$, if we take an H_2 column density of 10^{23} cm^{-2}. An appropriate value of dV/dR for Orion is uncertain, but, if we take $dV = 3$ km s^{-1} and $dR = 0.15$ pc (corresponding to 1′, the approximate width of the extended ridge source), then we estimate $x = X/(dV/dR) \approx 8 \times 10^{-11}$ km^{-1} s pc in this source. Figure 2*a* shows that this value would be too small for the 21.6 GHz line to appear stronger than its 18.3 GHz counterpart.

TABLE 2

C_3H_2 TRANSITIONS

Frequency[a] (MHz)	Transition	Excitation (K)
18343.14.....	1_{10}–1_{01}	0.9
21587.40.....	2_{20}–2_{11}	9.7
27084.34.....	3_{30}–3_{21}	17.1
44104.79.....	3_{21}–3_{12}	15.8
46755.62.....	2_{11}–2_{02}	8.7
51841.41.....	1_{11}–0_{00}	2.5
82093.55.....	2_{02}–1_{11}	6.4
82966.21.....	3_{12}–3_{03}	13.7
85338.90.....	2_{12}–1_{01}	4.1
145089.63.....	3_{12}–2_{21}	13.7
150820.67.....	4_{04}–3_{13}	19.3
150851.90.....	4_{14}–3_{03}	17.0

[a] From Thaddeus, Vrtilek, and Gottlieb 1985.

Because of the variation with excitation conditions of the nature and intensities of these two lines, and their strength and widespread occurrence, they are of interest as diagnostic tools for the determination of physical conditions in molecular clouds. To illustrate this potential, Figure 3 shows schematically how the line intensities are predicted to vary relative to each other as $N(H_2)$ changes. The results are for $T_k = 10$ K and values of $x = 10^{-8}$ and 10^{-10} km^{-1} s pc in the radiative transfer model described in § III. For low-to-moderate densities, the 2_{20}–2_{11} line is in absorption against the microwave background. For $N(H_2) \gtrsim 10^5$ cm^{-3}, depending upon the value of x (i.e., the optical thickness and degree of radiative trapping), both lines are predicted to be in emission, and either one, or both, may be superthermally excited.

To date there have been no reports of the 2_{20}–2_{11} line detected in emission from a dark cloud. For $x = 10^{-9}$ km^{-1} s pc, which may be appropriate for TMC-1, the transition from absorption to emission should occur at an H_2 density of about 2×10^5 cm^{-3}. Cox, Güsten, and Henkel 1987 have reported this line in emission in the planetary nebula NGC 7027. This source is probably hotter than $T_k = 30$ K, and the results of

© American Astronomical Society • Provided by the NASA Astrophysics Data System

1989ApJ...337..306A

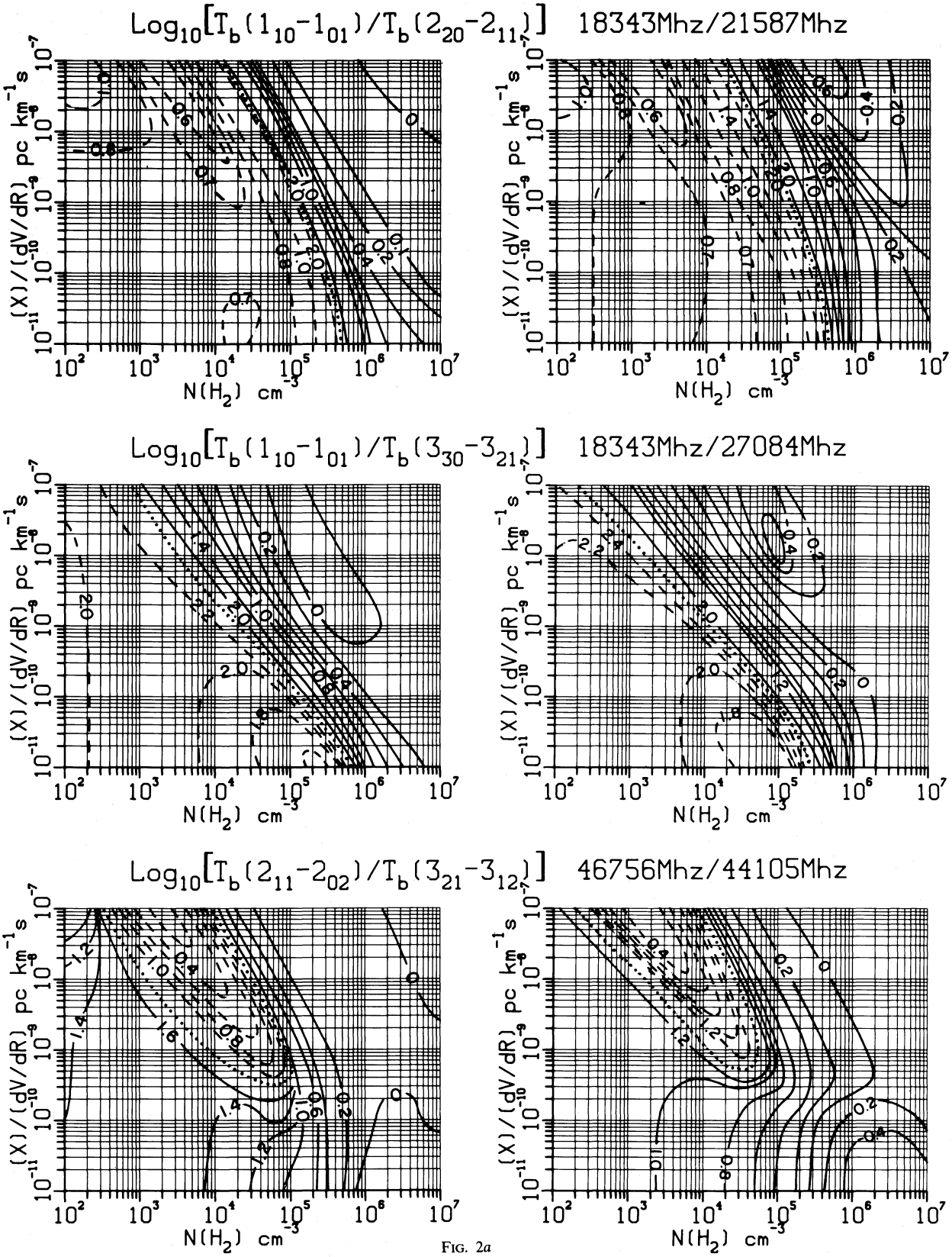

FIG. 2a

FIG. 2.—Contours of the logarithm (to base 10) of brightness temperature ratios for various C_3H_2 line pairs. The H_2 density is $N(H_2)$, X is the abundance of C_3H_2 relative to H_2, and dV/dR is the velocity gradient in the source. Plots on the left are for kinetic temperature, $T_k = 10$ K, those on the right for $T_k = 30$ K. The dotted line in each plot of (*a*) delineates regions of the $N(H_2)$–$X/(dV/dR)$ surface where the line in the denominator of the ratio is predicted to appear in absorption against the 2.8 K background. For the top four plots of (*a*) absorption occurs to the left of the dotted line; for the bottom two plots in (*a*) and (*b*) the absorption region is within the dotted line. Dashed contours indicate that the line in the denominator is in absorption.

© American Astronomical Society • Provided by the NASA Astrophysics Data System

1989ApJ...337..306A

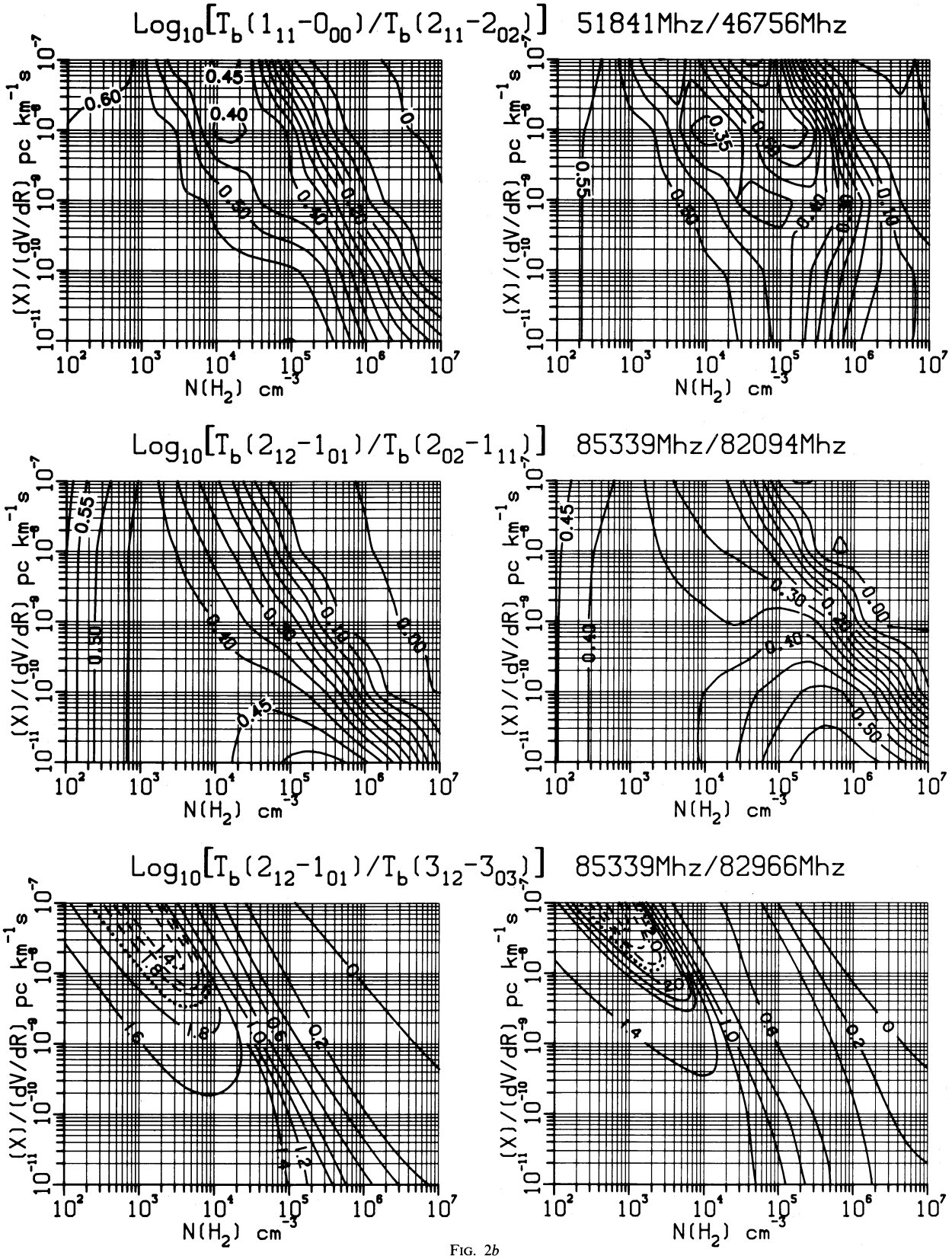

FIG. 2*b*

© American Astronomical Society • Provided by the NASA Astrophysics Data System

1989ApJ...337..306A

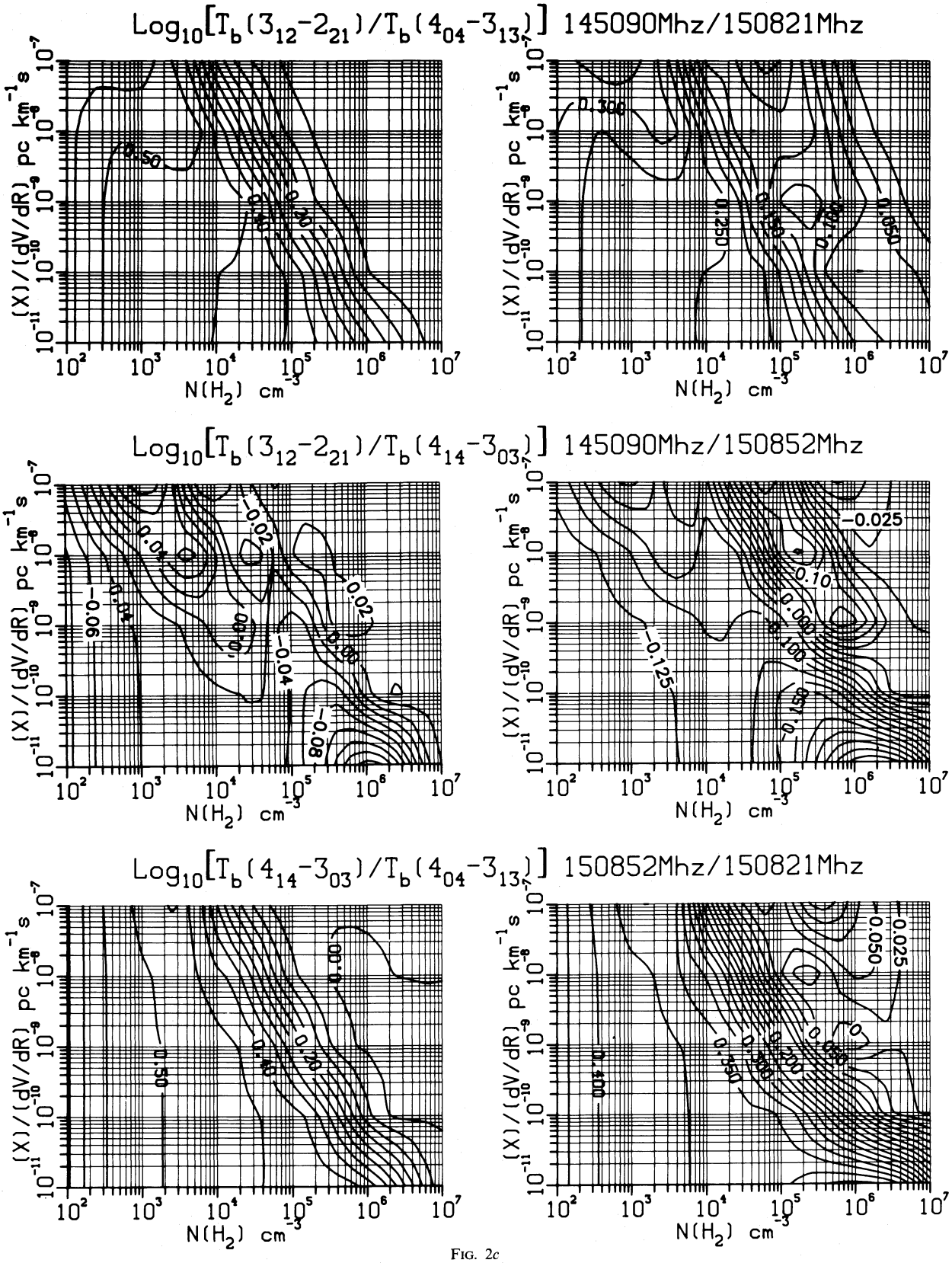

FIG. 2c

© American Astronomical Society • Provided by the NASA Astrophysics Data System

1989ApJ...337..306A

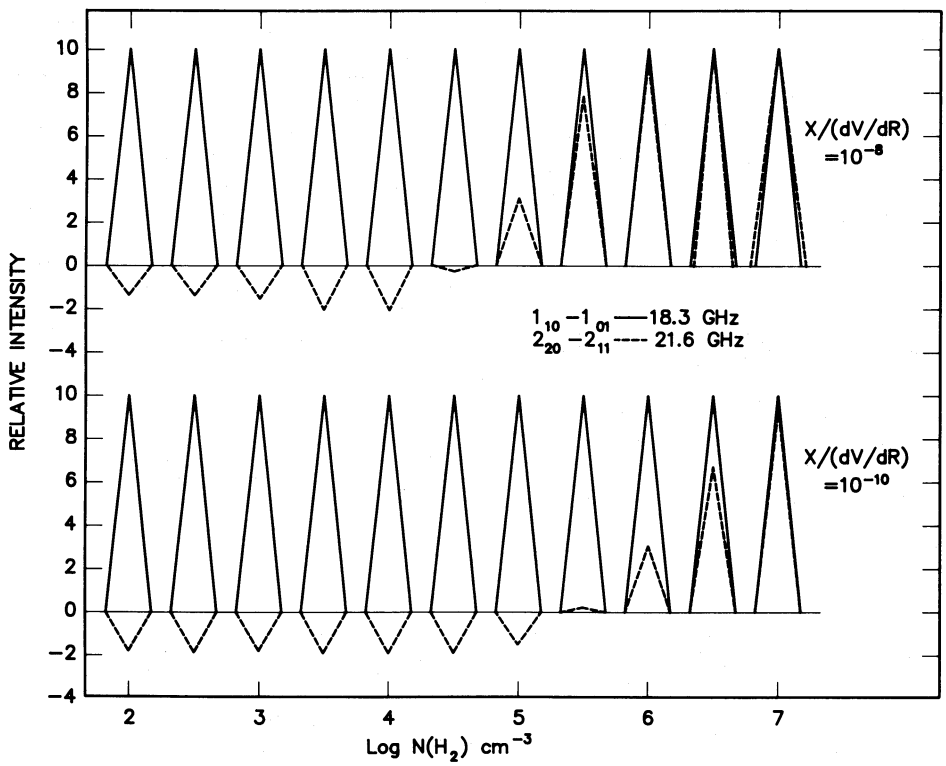

FIG. 3.—Schematic representation of the relative behavior of the 1_{10}–1_{01} and 2_{20}–2_{11} lines as a function of H_2 density for two values of $X/(dV/dR)$ in a cloud of $T_k = 10$ K. At each density the intensity of the stronger line is normalized to 10.

Figure 2*a* are therefore not directly applicable to these observations.

ii) 1_{10}–1_{01}, 3_{30}–3_{21} (18343 MHz, 27084 MHz)

In addition the 2_{20}–2_{11} line, two other transitions are predicted by our calculations to appear in absorption against the 2.8 K background under conditions which might be expected in molecular clouds. These are the 3_{30}–3_{21} and 3_{21}–3_{12} transitions, at frequencies of 27084 and 44105 MHz, respectively.

The middle frames of Figure 2*a* show how the ratio of the intensities of the 18.3 and 27.1 GHz lines is predicted to vary. In cold, dark clouds ($T_k = 10$ K), the 3_{30}–3_{21} line is predicted to be about 50–100 times weaker than the 1_{10}–1_{01} line over most of the density versus (abundance/velocity gradient) plane. For low-to-moderate densities, and depending somewhat on abundance, it should appear weakly in absorption, at about 1% the strength of the 1_{10}–1_{01} line.

To date the 27.1 GHz has not been looked for. The indications are that it will not be easy to detect. However, the 18.3 GHz line is very strong in some dark clouds, and line strengths of 1%–2% of the 1_{10}–1_{01} intensity correspond to tens of mK, a level which could be detected. The nature of such a detection, whether in emission or absorption and regardless of intensity, would be an interesting, rough indication of density.

The 30 K results shown in Figure 2*a* are qualitatively similar to those for 10 K, and the higher temperature increases the relative visibility of the 3_{30}–3_{21} line slightly at the higher densities.

iii) 2_{11}–2_{02}, 3_{21}–3_{12} (46756 MHz, 44105 MHz)

The range of parameters over which the 3_{21}–3_{12} line at 44.1 GHz is predicted to appear in absorption against the microwave background occupies the central part of the density versus (abundance/velocity gradient) plane in Figure 2*a*. By virtue of its excitation energy (16 K), the line is not likely to be very strong, especially in dark clouds. Madden *et al.* (1987) found $T_R^* = 1.8$ K in TMC-1 for the 2_{11}–2_{02} line, which indicates, based on the figure, that for typical dark cloud conditions the 3_{21}–3_{12} line should be observed (possibly in absorption) at $T_R^* \approx 0.12$ K in the strongest sources but, so far, attempts have been unsuccessful (Madden *et al.* 1987). For warmer clouds, where $X/(dV/dR)$ tends to be smaller because X is less (Bell *et al.* 1988), the 44.1 GHz line is likely to appear in emission against the 2.8 K background, if it is observable. Of course, the existence of background continuum, brighter than the 2.8 K, is common in warm sources, and could result in an absorption feature regardless of density or abundance.

iv) 1_{11}–0_{00}, 2_{11}–2_{02} (51841 MHz, 46756 MHz)

In spite of rather large atmospheric opacity, the 1_{11}–0_{00} line, at 51841 MHz, has been observed in TMC-1 by Madden *et al.* (1987) at FCRAO. Although the 2_{11}–2_{02} line at 46756 MHz is quite nearby in frequency, the steep gradient in atmospheric opacity at these frequencies means that calibration may be a problem in comparing these two lines. For $N(H_2) \approx 10^4$–10^5 cm^{-3}, Figure 2*b* predicts that the 1_{11}–0_{00} line should be 2.5 to 3 times stronger. But Madden *et al.* (1987) reported almost equal intensities. Whether this discrepancy should be attributed to modeling inadequacies or to calibration problems is not clear.

v) 2_{12}–1_{01}, 2_{02}–1_{11} (85339 MHz, 82094 MHz)

The 2_{12}–1_{01} line, at 85339 MHz, was first reported by Thaddeus, Guélin, and Linke (1981). It is easily observed in a variety of sources. The *para* 2_{02}–1_{11} line is weaker but is still rather

© American Astronomical Society • Provided by the NASA Astrophysics Data System

1989ApJ...337..306A

easily seen. For typical dark cloud parameters, the modeling predicts that the *ortho* line should be about twice as strong as the *para* line, in general agreement with the observations.

vi) 2_{12}–1_{01}, 3_{12}–3_{03} (85339 MHz, 82966 MHz)

The 3_{12}–3_{03} line, with an excitation temperature of 14 K, tends to be weaker in cold, dark clouds than the other two lines in this frequency range (Madden *et al.* 1987). The difference in excitation energies for these two lines results in a rather strong dependence upon $N(H_2)$ for the intensity ratio of this pair, particularly in cold clouds. For low density and optically thick conditions, the 3_{12}–3_{03} line may appear weakly in absorption against the 2.8 K background.

vii) 3_{12}–2_{21}, 4_{04}–3_{13} (145090 MHz, 150821 MHz)

These lines, and the 4_{14}–3_{03} transition, all have frequencies near 150 GHz, and low enough excitation energies that they should be observable in dark clouds. This line pair, particularly for $T_k = 10$ K, shows intensity ratios which are fairly strong functions of H_2 density for $N(H_2) \gtrsim 1 \times 10^4$ cm^{-3}. However, for densities below this, the contours of Figure 2*c* reveal a relatively flat surface.

viii) 3_{12}–2_{21}, 4_{14}–3_{03} (145090 MHz, 150852 MHz)

For both kinetic temperatures the intensity ratios of this combination form very flat surfaces (the contour intervals in Fig. 2*c* are 0.020 for 10 K and 0.025 for 30 K). Over the range of parameters which are likely to characterize most molecular clouds, the intensity ratio varies by $\pm 10\%$ or less for $T_k = 10$ K. Because observational uncertainties are likely to be of comparable magnitude, this combination is not likely to be of much use for diagnostic purposes. For $T_k = 30$ K, however, Figure 2*c* shows that somewhat greater variation occurs. The lines are predicted to be similar in intensity, with the model parameters affecting which one is actually stronger. This dependence of relative strength on conditions would help to compensate for the flat surfaces in the use of this pair for diagnostic purposes.

ix) 4_{14}–3_{03}, 4_{04}–3_{13} (150852 MHz, 150821 MHz)

The contoured surfaces in Figure 2*c* for these lines are qualitatively similar to those for the 3_{12}–2_{21}, 4_{04}–3_{13} pair. It seems that, for diagnostic purposes, both combinations are unnecessary for cold clouds. However, the similarity in frequency of these two lines will usually mean that they can be observed strictly simultaneously, an obvious advantage which makes this a useful pair for density diagnosis.

b) Application to Observations

The usefulness of C_3H_2 as a diagnostic tool will depend upon the realism with which the molecular clouds themselves can be physically modeled. An essential ingredient of the modeling is the collisional rate coefficients. It is difficult to assess with certainty the accuracy of the rates employed in the calculations for this paper, but indications are that they provide at least qualitative agreement with the observations, in predicting that the 2_{20}–2_{11} line should appear in absorption against the microwave background in cold, dark clouds.

In order to test the sensitivity of our results to uncertainty in the collisional rates, we have compared line strengths computed using both CS and the less accurate IOS rates. In general, the agreement is good, with differences of $\leq 20\%$ between computed T_{ex} values for most lines over the range of parameters expected for molecular clouds. Figure 4 shows the ratio of brightness temperatures calculated using the IOS and

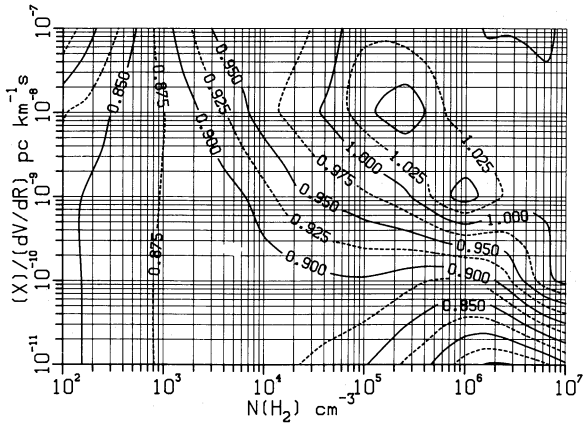

FIG. 4.—Ratio of IOS and CS calculations of brightness temperature of the 2_{12}–1_{01} line at 85339 MHz at a kinetic temperature of 30 K. (Note that, in contrast to Fig. 2, the ratio, not its logarithm, is plotted.)

CS rates at $T_k = 30$ K for the 2_{12}–1_{01} line at 85339 MHz. Other lines show qualitatively similar dependence upon the collisional rates. For this reason, even the relatively small uncertainties arising from the differences in rate coefficients will tend to disappear if the ratios of different lines, as in Figure 2, are used for diagnostic purposes.

A number of the lines referred to in Figure 2 have been observed in TMC-1 (Madden *et al.* 1987), and the observed line ratios can be compared with the computed ones to attempt an estimation of $N(H_2)$ and $X/(dV/dR)$ in this source. Each intensity ratio defines a locus of points in the appropriate 10 K diagram of Figure 2 which represents the set of $N(H_2)$, $X/(dV/dR)$ values which would produce the observed ratio. The intersection of two or more such loci would then define the values of these parameters for the cloud.

This procedure does not yield a particularly satisfactory result for TMC-1. For example, the 85.3, 82.1 GHz and 85.3, 83.0 GHz pairs, as observed by Madden *et al.* (1987), produce loci which do not actually intersect but run roughly parallel to each other, with closest approach in the vicinity of $N(H_2) = 7 \times 10^4$ cm^{-3} and $x = 2 \times 10^{-9}$ km^{-1} s pc. (The observed lines are strong, and rms noise levels in the data typically correspond to a few line widths in the plots of Fig. 2.) The observed ratio of the 51.8 and 46.8 GHz is approximately unity and cannot be fitted onto the plot of Figure 2*b*. The *K*-band lines at 18.3 and 21.6 GHz are clearly non-Gaussian, and the former shows evidence of self-absorption, which the modeling used in this paper does not permit. Given these uncertainties, there is not a clearly defined locus for this ratio on Figure 2*a*, but a range of parameters in the vicinity of $N(H_2) \approx 1 \times 10^4$ cm^{-3}, $x = (4\text{–}10) \times 10^{-9}$ km^{-1} s pc would be reasonably consistent with the observations. Thus, if we disregard the line pair near 50 GHz (which may be poorly calibrated because of strong differential atmosphere attenuation), the results indicate, for TMC-1, 10^4 cm^{-3} $\lesssim N(H_2) \lesssim 7 \times 10^4$ cm^{-3} and $2 \times 10^{-9} \lesssim x \lesssim 1 \times 10^{-8}$. Thus the observations, in comparison with Figure 2, do not yield particularly well-defined values for the parameters in TMC-1.

The most likely reason for this failure is the inadequacy of the radiative transfer model used in preparing Figure 2. The calculations utilized the LVG approximation for a homogeneous, spherical cloud undergoing uniform collapse. In fact,

© American Astronomical Society • Provided by the NASA Astrophysics Data System

1989ApJ...337..306A

TMC-1 (and most other quiescent dark clouds) does not possess large velocity gradients, is not obviously collapsing, and shows clear evidence of density structure (e.g., Snell, Langer, and Frerking 1982; Avery, MacLeod, and Broten 1982).

Radiative trapping effects are partly responsible for the differences in line-pair dependences in Figure 2. Consequently, inadequate or unrealistic modeling could account for the inconsistencies mentioned above. This explanation implies that use of the lines of C_3H_2 (or those of any other optically thick molecule) for diagnostic purposes requires a prior knowledge of the cloud structure in order that accurate modeling may be performed. This information will not, of course, be generally available, since it represents the goal of the exercise. Under such circumstances, an iterative approach, incorporating a number of degrees of freedom, and yielding a structure which may not be unique but is consistent with the data, may be the best solution possible.

V. SUMMARY AND CONCLUSIONS

The existence of a number of C_3H_2 line pairs, with the members of each pair close together in frequency but arising from states of different excitation energy, suggests that C_3H_2 may provide a useful means of estimating the H_2 density and relative C_3H_2 abundance in molecular clouds. The use of the brightness temperature ratios of such lines for diagnostic purposes largely eliminates systematic observational errors due to such factors as calibration, sky transmission, source coupling, and day-to-day variations. We have used the coupled states collisional excitation rates for C_3H_2, presented in this paper, to carry out statistical equilibrium calculations to assess the sensitivity of nine line pairs to changing physical conditions.

Of the various lines studied, four are predicted to be in absorption against the microwave background (i.e., $T_{ex} < 2.8$ K) over part of the density and optical thickness ranges which characterize molecular clouds. These are the 2_{20}–2_{11} (21587 MHz), 3_{30}–3_{21} (27084 MHz), 3_{21}–3_{12} (44105 MHz), and 3_{12}–3_{03} (82966 MHz) lines. Of these, the last one is predicted to be very weak in absorption (against the 2.8 K background) and is not likely to be observable except in emission, barring strong background sources. The 27.1 and 44.1 GHz lines are predicted to be relatively weak in dark clouds and have not yet been detected (though they may be observable), while the 2_{20}–2_{11} line has been observed in numerous cold, dark clouds, where it is always in absorption. The calculations indicate that, for sufficiently high density [$N(H_2) \gtrsim 10^4$ cm^{-3}, and depending upon C_3H_2 abundance], the 2_{20}–2_{11} line changes into emission ($T_{ex} > 2.8$ K), and it would be interesting to search for it with high spatial resolution in dense cloud cores where this prediction might be fulfilled. Cox, Güsten, and Henkel (1987) have reported the detection of the 2_{20}–2_{11} line in emission in the planetary nebula NGC 7027, which they characterize as having $T_k = 60$ K.

Of the various line pairs studied in this paper, the most useful, potentially, for diagnostic purposes appear likely to be (*a*) 1_{10}–1_{01}, 2_{20}–2_{11} (18343 MHz, 21587 MHz), (*b*) $2_{12}1_{01}$, 2_{02}–1_{11} (85339 MHz, 82094 MHz), (*c*) 2_{12}–1_{01}, 3_{12}–3_{03} (85339 MHz, 82966 MHz), and (*d*) 3_{12}–2_{21}, 4_{04}–3_{13} (145090 MHz, 150821 MHz) or 4_{14}–3_{03}, 4_{04}–3_{13} (150852 MHz, 150851 MHz). These lines are (or should be) among the strongest in C_3H_2 sources. The brightness temperature ratio emission character of pair *a* depends strongly upon $N(H_2)$, with the 2_{20}–2_{11} line changing from absorption against the 2.8 K background to emission as density increases.

The brightness ratio of pair *c* is also a strong function of density, especially for $T_k = 10$ K, varying by an order of magnitude for a density change of 10^4–10^5 cm^{-3} at $x = 10^{-8}$ km^{-1} s pc. The surfaces formed by the ratio contours for the two pairs of lines *d* are similar in shape, with the advantage of strictly simultaneous observations accruing to the 4_{14}–3_{03}, 4_{04}–3_{13} lines by virtue of their nearly equal frequencies.

The calculations of this paper are based for simplicity upon a spherical, homogeneous, uniformly collapsing cloud model, under the large velocity gradient approximation. Because this model is not likely to be suitable for many sources, the results of these studies should be taken as illustrative and applied rather circumspectly to actual data. For example, our preliminary attempts to deduce a density and abundance for TMC-1 from the observations of Madden *et al.* (1987), using the plots in Figure 2, did not yield particularly well-defined values. We attribute this failure primarily to the lack of a realistic model—one which would incorporate gradients in physical properties and departures from LVG radiative transfer.

The collisional excitation rates for C_3H_2 have been calculated using both the infinite-order sudden (IOS) (Green, DeFrees, and MacLean 1987) and the coupled states (CS) approximations for warm clouds (Green, DeFrees, and MacLean 1987) and for cold clouds (this paper). Calculations using both sets of rates for various C_3H_2 transitions at a kinetic temperature of 30 K indicate that the predicted line brightness temperatures generally agree to within better than 10% for the CS and IOS rates over the range of physical parameters appropriate for molecular clouds.

One of us (L. W. A.) would like to acknowledge helpful correspondence with Dr. Pierre Cox, which resulted in the detection of an error in an early version of the statistical equilibrium code used for this paper.

REFERENCES

Avery, L. W. 1987, in *IAU Symposium 120, Astrochemistry*, ed. M. S. Vardya and S. P. Tarafdar (Dordrecht: Reidel), p. 187.
Avery, L. W., MacLeod, J. M., and Broten, N. W. 1982, *Ap. J.*, **254**, 116.
Bell, M. B., Avery, L. W., Matthews, H. E., Feldman, P. A., Watson, J. K. G., Madden, S. C., and Irvine, W. M. 1988, *Ap. J.*, **326**, 924.
Bogey, M., Demuynck, C., Destombes, J. L., and Dubus, H. 1987, *J. Molec. Spectrosc.*, **122**, 313.
Brown, R. D., Godfrey, P. D., and Bettens, P. A. 1987, *M.N.R.A.S.*, **227**, 19P.
Cox, P., Güsten, R., and Henkel, C. 1987, *Astr. Ap.*, **181**, L19.
Goldreich, P., and Kwan, J. 1974, *Ap. J.*, **189**, 441.
Green, S. 1980, *Ap. J. Suppl.*, **42**, 103.
Green, S., DeFrees, D. J., and McLean, A. D. 1987, *Ap. J. Suppl.*, **65**, 75.
Kanata, H., Yamamoto, S., and Saito, S. 1987, *Chem. Phys. Letters*, **140**, 221.
Madden, S. C., Irvine, W. M., Matthews, H. E., and Avery, L. W. 1986, in *Proc. Workshop on Interstellar Processes* (NASA TM-88342) ed. D. J. Hollenbach and H. A. Thronson (Dordrecht: Reidel), p. 155.
Matthews, H. E., and Irvine, W. M. 1985, *Ap. J. (Letters)*, **298**, L61.
Matthews, H. E., Madden, S. C., Avery, L. W., and Irvine, W. M. 1986, *Ap. J.(Letters)*, **307**, L69.
Seaquist, E. R., and Bell, M. B. 1986, *Ap. J. (Letters)*, **303**, L67.
Snell, R. L., Langer, W. D., and Frerking, M. A. 1982, *Ap. J.*, **225**, 149.
Thaddeus, P., Guélin, M., and Linke, R. A. 1981, *Ap. J. (Letters)*, **246**, L41.
Thaddeus, P., Vrtilek, J. M., and Gottlieb, C. A. 1985, *Ap. J. (Letters)*, **229**, L63.

LORNE AVERY: Herzberg Institute of Astrophysics, National Research Council of Canada, 100 Sussex Drive, Ottawa, Ontario K1A 0R6, Canada

SHELDON GREEN: NASA Institute for Space Studies, 2880 Broadway, New York, NY 10025

© American Astronomical Society • Provided by the NASA Astrophysics Data System